Cyclotron Resonance Studies of the Fermi Surfaces in Bismuth

YI-HAN KAO
IBM Watson Research Laboratory, Columbia University, New York
(Received 10 September 1962; revised manuscript received 4 October 1962)

Experiments on cyclotron resonance of the Azbel'-Kaner type were performed on pure Bi at 34.5 kMc/sec. Angular variation of the cyclotron masses for both the electrons and the holes with the magnetic field in the binary, bisectrix, and trigonal planes were studied. For the electrons in Bi, the tilt angle of the Fermi surface in the crystallographic coordinate system was directly measured. The mass parameters in Cohen's nonellipsoidal-nonparabolic model were determined for the first time. The inverse effective mass tensor components in Shoenberg's ellipsoidal-parabolic model were completely determined by using the tilt angle. The results indicate that the ellipsoidal-parabolic model is unable to explain quantitatively all the angular variation in the electron cyclotron masses. One particular case of Cohen's model corresponding to electron Fermi surfaces at centers of the six pseudohexagonal faces of the Brillouin zone was shown to be in better agreement with the experimental results. Angular variation of the light-hole cyclotron masses with field in the three crystallographic planes were fitted quite satisfactorily by the one-spheroid model. No resonance of a heavy hole was observed in this experiment.

I. INTRODUCTION

CYCLOTRON resonance provides a useful tool for exploring the Fermi surface in metals. For a given direction of the external magnetic field H, measurements of the cyclotron mass $m^*=(1/2\pi)(\partial a/\partial E)$ at resonance give the energy derivative of the extreme cross-sectional area of the Fermi surface in momentum space perpendicular to H. The details of angular variation of m^* can be conveniently used in conjunction with other information to establish the shape of the Fermi surface.

Early studies[1–4] have demonstrated that the Fermi surface for electrons in bismuth can be satisfactorily described by a set of equivalent ellipsoids in momentum space with one axis in common with the binary axis and the other two axes being tilted several degrees from the trigonal and bisectrix axes. Recently, both experimental[5,6] and theoretical[7] work have indicated that these Fermi surfaces may not be ellipsoidal-parabolic, so that m^* is energy-dependent and one needs more parameters to specify one "ellipsoid."

The de Haas-van Alphen (dHvA) effect[4,8] and cyclotron resonance[9–13] have been observed in bismuth. The extreme cross-sectional area of the Fermi surface and their energy derivatives measured by these experiments, if completed for all orientations, enable one to map out the topology of the Fermi surface. To date, however, all these measurements have been done with H along the crystallographic axes or in the trigonal plane. These results are by no means complete in themselves. Furthermore, all of the previous data were interpreted by using Shoenberg's ellipsoidal-parabolic model; one usually multiplies the dHvA period by the cyclotron mass to get the Fermi energy. For a nonellipsoidal-nonparabolic Fermi surface, this traditional procedure of obtaining the Fermi energy is incorrect and has led to confusion.

In the present work, angular variation of the cyclotron masses for both electrons and holes with H in the binary, bisectrix, and trigonal planes were studied. The tilt angle of the electron Fermi surface in the crystallographic axis system was directly measured without having to extrapolate by using the ellipsoidal-parabolic (EP) model as was done in all previous work. These results, combined with values of the Fermi energy and the thermal energy gap recently measured by other experiments,[6,14] enable us to obtain all the parameters in Cohen's nonellipsoidal-nonparabolic (NENP) model[7] and thus to completely specify the Fermi surface for the carriers we have observed.

II. FERMI SURFACES IN BISMUTH

1. Electrons

Shoenberg's extensive work[4,8] on the dHvA effect have shown that one of the elliposids (ellipsoid I) can be described in the crystallographic axis system by

$$2m_0E=\mathbf{p}\cdot\boldsymbol{\alpha}\cdot\mathbf{p}, \tag{1}$$

where

$$\boldsymbol{\alpha}=\begin{bmatrix}\alpha_{xx} & 0 & 0\\ 0 & \alpha_{yy} & \alpha_{yz}\\ 0 & \alpha_{zy} & \alpha_{zz}\end{bmatrix} \tag{2}$$

is the inverse effective mass tensor, m_0 the free-electron mass, E the energy, and $\mathbf{p}$ is the quasi-momentum. The

[1] H. Jones, Proc. Roy. Soc. (London) **A147**, 396 (1934).
[2] D. Shoenberg and M. Zaki Uddin, Proc. Cambridge Phil. Soc. **32**, 499 (1936); Proc. Roy. Soc. (London) **A156**, 701 (1936).
[3] M. Blackman, Proc. Roy. Soc. (London) **A166**, 1 (1938).
[4] D. Shoenberg, Proc. Roy. Soc. (London) **A170**, 341 (1939); Phil. Trans. Roy. Soc. (London) **A245**, 1 (1952).
[5] B. Lax, Bull. Am. Phys. Soc. **5**, 167 (1960).
[6] B. Lax, J. G. Mavroides, H. J. Zeiger, and R. J. Keyes, Phys. Rev. Letters **5**, 241 (1960).
[7] M. H. Cohen, Phys. Rev. **121**, 387 (1961).
[8] D. Shoenberg, *Progress in Low Temperature Physics* (North-Holland Publishing Company, Amsterdam, 1957), Vol. II.
[9] J. K. Galt, W. A. Yager, F. R. Merritt, B. B. Celtin, and H. W. Dail, Jr., Phys. Rev. **100**, 748 (1955).
[10] R. N. Dexter and B. Lax, Phys. Rev. **100**, 1216 (1955).
[11] J. E. Aubrey and R. G. Chambers, J. Phys. Chem. Solids **3**, 128 (1957).
[12] J. E. Aubrey, J. Phys. Chem. Solids **19**, 321 (1961).
[13] J. K. Galt, W. A. Yager, F. R. Merritt, B. B. Celtin, and A. D. Brailsford, Phys. Rev. **114**, 1396 (1959).
[14] D. Weiner, Phys. Rev. **125**, 1226 (1962).

other two ellipsoids (ellipsoids II and III) are generated by rotating (1) through $\pm 120°$ about the trigonal (z) axis. Cyclotron masses derived from this model can be found in reference 8.

In Cohen's NENP model, as judged from the band calculation of Mase[15] and Harrison[16] and the recent analysis by Jain and Koenig,[17] one of the Fermi surfaces for electrons can be expressed, in Cohen's notation (with $m_2'=m_2$),[6,14] by

$$\frac{p_1^2}{2m_1}+\frac{p_2^2}{2m_2}+\frac{p_3^2}{2m_3}=E\left(1+\frac{E}{E_g}\right)-\left(\frac{p_2^2}{2m_2}\right)^2\frac{1}{E_g}, \quad (3)$$

where 1, 2, 3 refer to the principal axis system of the ellipsoid, the m's are the effective masses at the bottom of the conduction band, and E_g is the energy gap. Expressions for cyclotron masses derived from (3) are given in Appendix A.

2. Holes

From the $\mathbf{k}\cdot\mathbf{p}$ approximation and by analogy with the conduction band of germanium, it seems reasonable to expect the valence band to be parabolic. Jones[1] first suggested such a model for the hole Fermi surface which can be represented by

$$2m_0E_h=\beta_1p_x^2+\beta_2p_y^2+\beta_3p_z^2, \quad (4)$$

where E_h is the hole Fermi energy and the β's are components of the hole inverse effective mass tensor. As is shown later, in contrast to the large uncertainties encountered by Brandt *et al.*,[18] this model (with $\beta_1=\beta_2$) agrees with our results very closely.

Probable locations of these Fermi surfaces in the Brillouin zone are shown in Fig. 1.

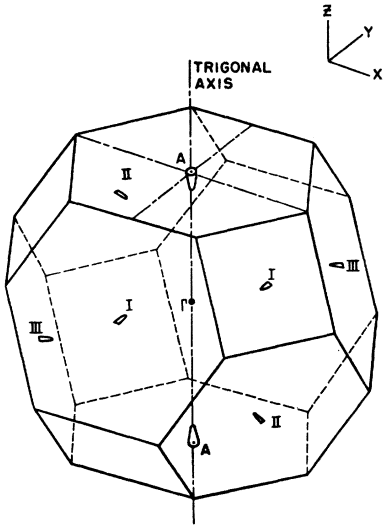

FIG. 1. Probable locations of Fermi surfaces in the Brillouin zone. The six half-elliposids for electrons are designated by I, II, III at the centers of the six pseudohexagonal faces. The two half-elliposids for light holes are at points A, centers of the two perfect hexagonal faces.

III. EXPERIMENTAL

1. Sample Preparation

Zone-refined pure bismuth was obtained from the Consolidated Mining and Smelting Company of Canada, Ltd. Single crystals of the required orientation were grown on a hot plate by a seeding technique. Good single crystals of sizes about 25 mm×15 mm×5 mm obtained by this method were then cut into a size of about 15 mm×15 mm×5 mm suitable for the experiment by a spark cutter or by a high-speed abrasive wheel with reasonably slow cutting rate. Preliminary crystal orientation was determined by cleaving in liquid nitrogen followed by etching in 35% HNO_3. This sample surface was then electrolytically polished using the method given by Tegart.[19] The sample was finally examined by x rays to ensure that it be strain free and of the required crystal orientation. Single crystals of similar size grown by the same method have been reported[20] with residual resistance ratios of about 400 between 300 and 4°K.

2. Experimental Apparatus

The experiment was performed with standard microwave technique at frequencies near 35 kMc/sec. Variation of surface resistance as a function of H was observed by detecting the change in Q of a rectangular cavity of which the Bi sample serves as the bottom wall. The cavity and the sample were immersed in liquid helium, the temperature of the liquid helium was lowered to below the λ-point so that the disturbance due to bubbling at the liquid surface was suppressed. The microwave power from a stabilized klystron was branched at a magic tee, and part of the power was transmitted to the cavity while the other part was fed into a matched load. The reflected power from the cavity was detected in the fourth arm of the magic tee by a crystal detector. The magnetic field was measured by a Bell model 120 gaussmeter using a Hall-effect probe.

During the experiment, the temperature of the liquid helium was reduced to around 1.5°K by pumping, and when equilibrium had been reached, the frequency of the klystron output was tuned to the frequency of the cavity resonance and stabilized by an automatic frequency control unit suggested by Kip.[21] The output voltage of the crystal detector was fed into a Keithley

[15] S. Mase, J. Phys. Soc. Japan **13**, 434 (1958); **14**, 584 (1959).
[16] W. A. Harrison, J. Phys. Chem. Solids **17**, 171 (1960).
[17] A. L. Jain and S. H. Koenig, Phys. Rev. **127**, 442 (1962).
[18] N. B. Brandt, A. E. Dubrovskaya, and G. A. Kytin, Soviet Phys.—JETP **10**, 405 (1960).
[19] W. J. Tegart, *The Electrolytic and Chemical Polishing of Metals in Research and Industry* (Pergamon Press, Inc., London, 1959).
[20] A. N. Friedman and S. H. Koenig, IBM J. Research Develop. **4**, 158 (1960).
[21] We are indebted to Professor A. F. Kip for this private communication.

model 150AR microvolt-ammeter which was used as a chopper amplifier. As the magnetic field was swept, the output voltage of the microvolt-ammeter and of the gaussmeter were used to drive an X-Y recorder.

IV. RESULTS AND DISCUSSION

For a metal under anomalous skin-effect conditions, Azbel' and Kaner[22] have shown that the surface impedance can be expressed as

$$Z(H)=R(H)+iX(H)=Z(0)\ (1-e^{-2\pi i\omega/\omega_c}e^{-2\pi/\omega_c\tau})^{1/3}. \quad (5)$$

In the derivation of this basic equation, it has been assumed that (i) the carriers obey the quadratic dispersion law and (ii) $\delta \ll r$, l, where r is the radius of the Larmor orbit, l the mean free path of the carriers, and δ is a skin depth. The surface impedance is a minimum at resonance, i.e., when $\omega=n\omega_c$, n being a nonzero integer. When condition (i) is not fulfilled, a resonance can only be observed at extremal values of ω_c which in this case is a function of momentum. The condition (ii) is well satisfied in most metals at liquid-helium temperature. But in the case of Bi, even though $\delta \ll l$ at low temperatures, the requirement that $\delta \ll r$ can easily be violated at moderate magnetic fields. For Bi, we can take $p\sim 10^{-21}$ g-cm-sec^{-1}, $\delta\sim 10^{-4}$ cm, $r=pc/eH$, and then we get $r\sim\delta$ for H of the order of several hundred gauss. Thus, Eq. (5) will give only a qualitative picture of the phenomenon for Bi as was considered by Azbel' and Kaner.[23] Nevertheless, we would expect Eq. (5) to hold at very low magnetic fields and the classical conditions to be predominant in the high-field region. Unfortunately, since for Bi many resonances occur in the intermediate range of fields, neither extreme case by itself completely describes the behavior of the surface impedance.

In a moderatly high field region, we can construct a simple model to explain the behavior of the surface impedance. Let us divide the electrons into two groups: those whose orbits are within the skin depth, and another group whose orbits are centered at a depth $\sim r$ below the skin depth. The first group of electrons behave more or less classically since they remain within the skin depth and do not give rise to a significant resonance-like behavior of the surface impedance. The second group of electrons spend only a small fraction of their orbiting time within the skin depth, and can

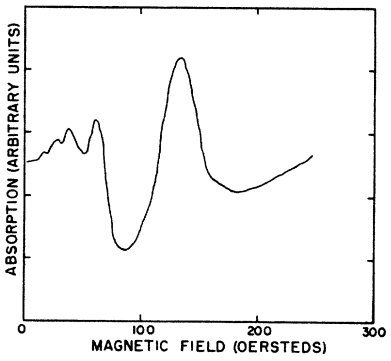

FIG. 2. Power absorption vs magnetic field with the magnetic field directed along the binary axis and perpendicular to the microwave electric field.

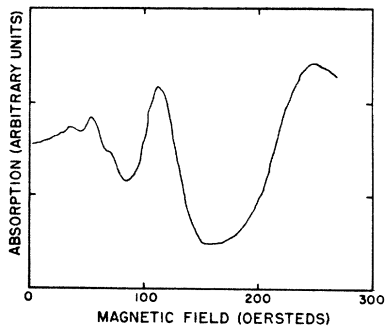

FIG. 3. Power absorption vs magnetic field with the magnetic field directed along the bisectrix axis and perpendicular to the microwave electric field.

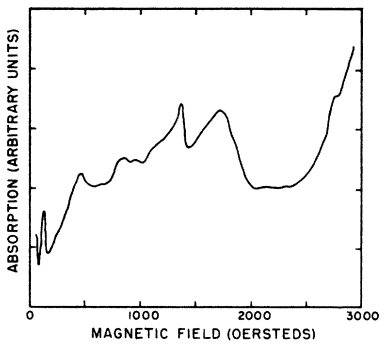

FIG. 4. Power absorption vs magnetic field with the magnetic field directed along the binary axis and perpendicular to the microwave electric field.

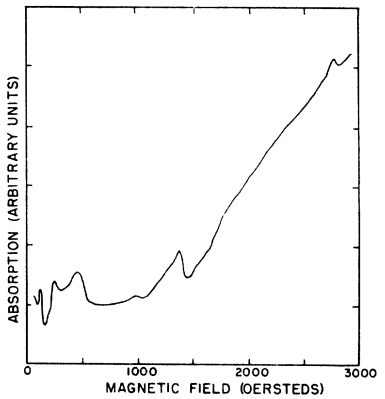

FIG. 5. Power absorption vs magnetic field with the magnetic field directed along the bisectrix axis and perpendicular to the microwave electric field.

[22] M. Ia. Azbel' and E. A. Kaner, Soviet Phys.—JETP **3**, 772 (1956); **5**, 730 (1957).

[23] M. Ia. Azbel' and E. A. Kaner, J. Phys. Chem. Solids **6**, 113 (1958).

be considered to be described by the anomalous conditions, and it is this group which is primarily responsible for the oscillatory behavior of the surface impedance predicted by (5). As the magnetic field is increased, the number of the classically behaving electrons increases while that of the other electrons decreases. Thus, over some region of fields, the surface impedance passes from the anomalous conditions to the classical conditions. It must be remembered that δ varies with the magnetic field and thus an exact analysis of the behavior of the surface impedance with magnetic field is considerably more complicated.

The situation is further complicated when more than one type of carriers is present and gives rise to interference in oscillations of the surface impedance. In this case, it is difficult to apply the Azbel'-Kaner theory to the experimental results even in the low-field region.

Typical experimental curves of power absorption, which is proportional to the surface resistance, are

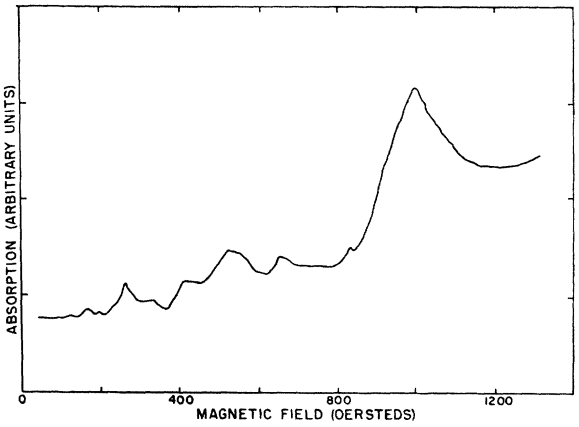

FIG. 6. Power absorption vs magnetic field with the magnetic field directed along the trigonal axis and perpendicular to the microwave electric field.

shown in Figs. 2–6. Measurements were done at $T\sim1.5$°K and at a microwave frequency 34.5 kMc/sec with an $\omega\tau$ estimated to be 20. It can be seen that periodic oscillations occur at low fields with the shape resembling those predicted by (5) (Figs. 3 and 7). For H higher than ~200 G, the oscillatory behavior becomes complicated probably because of the physical argument given above. It has been found experimentally[11,12] that many maxima in the absorption curve are better defined than the minima, as is also seen in our data. If we use the positions of the maximum in power absorption to identify the resonances, we can find many subharmonics in a series of peaks. Without a theory giving the quantitative behavior of the surface impedance in Bi over the whole range of magnetic fields, we adopt the same criterion to obtain the cyclotron masses as was used by Aubrey and Chambers.[11] Cyclotron masses are obtained either from the fundamental peak (first maximum in a series) or by averaging over the periods of oscillation when a long series is observed.

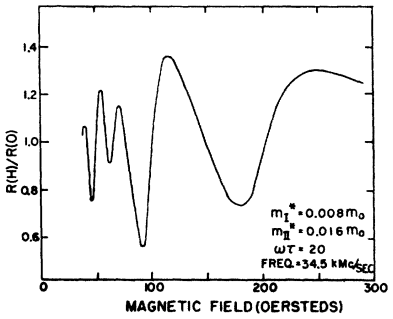

FIG. 7. Plot of $R(H)/R(0)$ vs H for two independent carriers using (5) with $Z(0)=2R(0)\exp(i\pi/3)$.

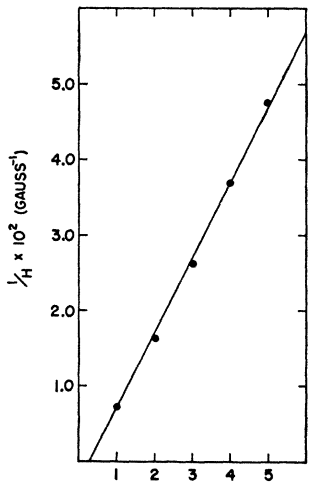

FIG. 8. Values of $1/H$ for the maxima in the power absorption curve of Fig. 2 vs successive integers.

For example, from Fig. 2 we obtain five peaks in the low-field region for a magnetic field parallel to the binary axis. These maxima occur at $H=134.2$, 61.8, 38, 27.1, 21 G; they are identified as the series of fundamental and subharmonics of the electron resonance, with $n=1$, 2, 3, 4, 5, respectively. If we plot $1/H$ vs the integer n, we should get a straight line of slope $e/m^*\omega c$. This plot is shown in Fig. 8. From the slope we have determined $m^*=0.0107m_0$. This is the case when there is only one cyclotron mass involved. However, it is frequently observed in the experiment that several masses are present in the same curve, in which only one or two subharmonics can be identified for each mass. In those cases, the position of the fundamental peak instead of the slope of the straight line is used to determine m^*. This procedure of identification may lead to a systematic error in m^* by as much as 20%.

However, in the case when the angular variation of m^* calculated from certain models are compared with that observed in this experiment, the mass parameters in the different models are determined from the same observed maxima in the power absorption curve for H along some particular directions. Based upon the as-

sumption that the systematic error in m^* is presumably insensitive to the angular variation, comparison of calculated and observed values of m^* for H in the other directions are then essentially subject to the random experimental errors, which are estimated to be around a few percent. Thus, although the absolute uncertainty in mass determination is large, comparison of angular variation can still be made with reasonable accuracy provided all the points to be compared are determined by the same criterion.

For each given relative orientation of the bismuth crystal and the dc magnetic field H, linearly polarized microwave fields are set at two different directions, one with $H \perp E_{rf}$ and one with $H \perp H_{rf}$. No significant change in either the position or the intensity of the resonance lines was observed in our experiment by measuring the power absorption. This is in contrast to the case of copper,[24] in which the resonances are largely due to the stationary orbits and there is a change in the intensity of absorption with two different directions of polarization. Another possibility is that mode mixing takes place in the resonant cavity. Since the bismuth crystal is anisotropic, linearly polarized waves become elliptically polarized in the cavity and the effect due to different linear polarizations is washed out.

The fact that there is no change in the intensity of the resonance lines also indicates that electron spin resonance and combined resonance[25] were not observed since these resonances occur only with $H \perp H_{rf}$. Failure to observe these two types of resonance is presumably due to insufficient sensitivity in our experimental arrangement.

We now consider the following cases.

1. H in the Binary Plane

A. Electrons

Since $\alpha_{yz}=\alpha_{zy}$ are the only nonvanishing off-diagonal components of the inverse effective mass tensor, the principal axis (123) system is generated from the crystallographic (xyz) system by a rotation through an angle θ_t about the binary (x) axis; θ_t is the tilt angle. Hence for H in the binary plane, the angular dependence of m^* in the principal axis system differs from that in the xyz system only by a constant angle of rotation; the cyclotron mass is a maximum when H is parallel to axis 3 and a minimum when H is parallel to axis 2.

In the EP model, when H is in the binary plane, ellipsoids II and III always give the same cyclotron masses. Thus, in general, there are two cyclotron masses due to all the electron ellipsoids. When H is parallel to the trigonal axis, these masses become degenerate. In the previous work on cyclotron resonance,[11–13] the value of m^* for H parallel to the trigonal axis is used as one of the four conditions to determine the mass parameters. In our case, in order to make a convenient comparison of the EP model with the NENP model, we replace this condition by the value of m^* for H parallel to axis 3. Moreover, without relying on data from other experiments, we use the measured tilt angle to be the fourth condition.

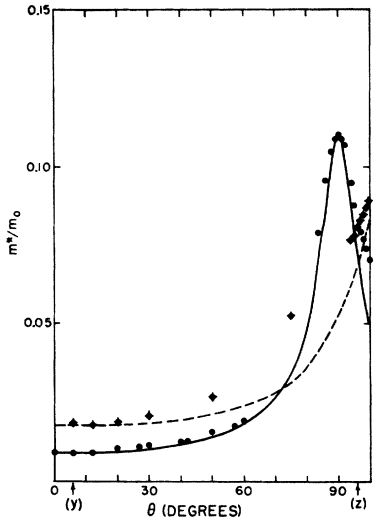

FIG. 9. Angular variation of the electron cyclotron masses with H in the binary plane. θ is the angle between H and axis 2. Directions of the bisectrix (y) axis and the trigonal (z) axis are indicated by arrows. Solid curve is the angular variation of $m_{\rm I}^*$ calculated from the NENP model by using (A8) and the mass tensor components determined in (19). Dashed curve is the angular variation of $m_{\rm II}^*$ ($=m_{\rm III}^*$) calculated from the EP model using (1) and (15).

The observed angular variation of m^* for electron is indicated by points in Fig. 9. We identify axis 3 and the trigonal axis, respectively, by observing through rotation of H in the binary plane the directions along which m^* is maximum and along which all the electron cyclotron masses become degenerate. We measure the angle between these two directions to be 6°; this is in close agreement with the value 5.7° obtained by Shoenberg.[4,8] The accuracy in determining the tilt angle is primarily limited by one's ability to prepare crystals of the required orientation.

The following results obtained with H in the binary plane are used to determine the effective masses:

$$H \text{ along principal axis 2:} \quad m_2^*=0.009\pm0.0009m_0, \tag{6}$$

$$H \text{ along principal axis 3:} \quad m_3^*=0.11\pm0.01m_0, \tag{7}$$

$$\theta_t=6°\pm0.2°. \tag{8}$$

In analyzing the data, the angular variation of m^* calculated from the EP model using the mass parameters given by Galt *et al.*[13] was used as a guide to select the cyclotron masses and to associate them with the corresponding ellipsoids. This method was used to obtain the points shown in Fig. 9. However, for "ellipsoids" II and III, the deviation from the EP model is large beyond the region shown by Fig. 9 and the structure of the power absorption curve is complicated by the presence of

[24] A. F. Kip, D. N. Langenberg, and T. W. Moore, Phys. Rev. **124**, 359 (1961).

additional peaks probably due to spin resonance absorption or dielectric anomalies. Identification of m^* for these two "ellipsoids" becomes very difficult. At the present time, no attempt has been made to definitely identify these absorption peaks beyond the region which we have plotted in Fig. 9. Of course, a calculation of the angular variation using the NENP model may serve as a guide to resolve this question, but as we see later, the complexity of the electron Fermi surface in the NENP model indicates that an analytical calculation of this entire angular variation is almost impossible.

For H parallel to the binary axis, we have found that

$$m_1^*=0.14\pm0.02m_0. \tag{9}$$

With the values given in (6) to (9), we can determine all the mass parameters in the EP model (1) and in the NENP model (3) when appropriate values of E and E_g are used.

We consider the EP model first. In the principal axis system, components of the inverse effective mass tensor are given by

$$\begin{aligned}\alpha_1&=m_1^*/m_2^*m_3^*,\\ \alpha_2&=m_2^*/m_3^*m_1^*,\\ \alpha_3&=m_3^*/m_1^*m_2^*.\end{aligned} \tag{10}$$

In the crystallographic axis system it can be shown that

$$\begin{aligned}\alpha_{xx}&=\alpha_1,\\ \alpha_{yy}&=\alpha_2\xi^2+\alpha_3\eta^2,\\ \alpha_{zz}&=\alpha_2\eta^2+\alpha_3\xi^2,\\ \alpha_{yz}&=(\alpha_3-\alpha_2)\xi\eta,\end{aligned} \tag{11}$$

where

$$\xi=\cos\theta_t, \quad \eta=\sin\theta_t. \tag{12}$$

From Eqs. (6)–(12), we obtain the following values for the EP model:

$$\alpha_1=141, \quad \alpha_2=0.584, \quad \alpha_3=87.3, \tag{13}$$

$$m_1=0.00709m_0, \quad m_2=1.71m_0, \quad m_3=0.0115m_0, \tag{14}$$

$$\alpha_{xx}=141, \quad \alpha_{yy}=1.53, \quad \alpha_{zz}=86.3, \quad \alpha_{yz}=9.01. \tag{15}$$

In the NENP model, m^* is given by (A8) for H in the binary plane. From this expression, we get H along axis 2:

$$m_2^*=(1+2E/E_g)(m_1m_3)^{1/2}. \tag{16}$$

H along axis 3:

$$m_3^*=(2/\pi)(1+2E/E_g)(m_1m_2/2)^{1/2}G(0). \tag{17}$$

Applying (A10), we obtain:

H along axis 1:

$$m_1^*=(2/\pi)(1+2E/E_g)(m_2m_3/2)^{1/2}F(0). \tag{18}$$

From Eqs. (16)–(18), using Weiner's value[14] of $E/E_g=0.50$, Eqs. (6)–(9), and $F(0)=G(0)=1.686$, we determine the following values for the NENP model at the bottom of the conduction band:

$$m_1=0.00354m_0, \quad m_2=1.49m_0, \quad m_3=0.00573m_0, \tag{19}$$

$$\alpha_1=282, \quad \alpha_2=0.671, \quad \alpha_3=175, \tag{20}$$

$$\alpha_{xx}=282, \quad \alpha_{yy}=2.58, \quad \alpha_{zz}=173, \quad \alpha_{yz}=18.1. \tag{21}$$

It can be seen from Eqs. (16)–(18) that the cyclotron masses at the bottom of the conduction band are about half the cyclotron masses at the Fermi energy. In the EP model, E/E_g is assumed to be negligible, thus when the cyclotron masses measured at the Fermi energy are used to determine the effective masses at the bottom of the hand, a factor of 2 is introduced on the effective masses m_1 and m_3 [comparing (14) with (19)].

With values given in (19) and $E/E_g=0.50$, we apply (A8) to calculate the angular variation of m^* for "ellipsoid" I with H in the binary plane. The result is given by the solid line in Fig. 9. Agreement with the experimental result is seen to be fairly good. In this plot, the cyclotron masses for H along axis 3 and axis 2 are chosen to fit the experimental points. The deviation of the experimental values from the calculated curve in the neighborhood of axis 3 may be either due to crystal misorientation or to approximations in the theory or our calculation.

In order to compare the NENP model and the EP model in the present case, we have calculated the angular variation of m^* in the EP model using the values given in (13). From the EP model (1), it can be shown[8] that

$$m^*/m_0=(\cos^2\theta\alpha_1\alpha_3+\sin^2\theta\alpha_1\alpha_2)^{-1/2}. \tag{22}$$

Here θ is the angle between H and axis 2 in the principal axis system.

Values of m^* calculated from both models are listed in Table I. It should be noted that measured values of m^* at $\theta=0°$ and $\theta=90°$ are used to deduce the α's which in turn are used to calculate the angular variation of m^*. We see that both models yield the same cyclotron masses except in a region close to axis 3, where the values obtained from the EP model are *smaller* by $\sim7\%$. When comparing these calculated values with the experimental points as shown in Fig. 9, we notice that in the

TABLE I. Angular variation of m^*/m_0 for the "ellipsoid" I with H in the binary plane calculated from the EP and the NENP models. θ = angle between H and axis 2. Values at $\theta=0°$ and $\theta=90°$ in both models are chosen to fit the experimental data.

θ	m^*/m_0 from EP model	m^*/m_0 from NENP model
0°	0.009	0.009
10°	0.092	0.092
30°	0.0104	0.0104
50°	0.014	0.014
60°	0.0178	0.0180
70°	0.0257	0.0260
80°	0.0469	0.0486
85°	0.0752	0.080
90°	0.11	0.11

region where these two models do not agree, the experimental results reveal better agreement with the NENP model although the fitting is not perfect.

In order to obtain m^* for "ellipsoids" II and III from the NENP model, one has to perform rotations of (3) through $\pm 120°$ about z axis in the crystallographic (xyz) system which differs from the principal axis (123) system by a rotation of θ_t about axis 1. The presence of the term containing p_2^4 complicates the expression for the Fermi surface under these rotations. In the (xyz) system, (3) becomes

$$\frac{(p_y^4\xi^4+p_z^4\eta^4+6p_y^2p_z^2\xi^2\eta^2-4p_y^3p_z\xi^3\eta-4p_yp_z^3\xi\eta^3)}{(2m_2E_g)^2}$$
$$+\frac{p_1^2}{2m_1E_g}+\frac{p_y^2\xi^2+p_z^2\eta^2-2p_yp_z\xi\eta}{2m_2E_g}$$
$$+\frac{p_y^2\eta^2+p_z^2\xi^2+2p_yp_z\xi\eta}{2m_3E_g}=\frac{E}{E_g}\left(1+\frac{E}{E_g}\right). \quad (23)$$

From this equation, an analytical form for m^* with H in an arbitrary direction seems almost impossible to obtain.

We thus used the EP model to calculate m^* for ellipsoids II and III with H in the binary plane. This was done by rotations of (1) using the values determined in (15) (appropriate formulas can be found in reference 8). The results are plotted as the dashed curve in Fig. 9. When compared with the observed values of m^* which are identified as belonging to these two ellipsoids, we see that experimental points agree with the dashed curve only in the vicinity of the bisectrix (y) axis. In other directions, the values given by the EP model are too small.

B. Holes

When H is in a direction near the trigonal axis, the hole cyclotron mass is nearly equal to the electron cyclotron mass. Thus, for the Azbel'-Kaner type resonance, it will be difficult to select the right mass with H parallel to the trigonal direction. We, thus, start with H along the bisectrix axis, since for H along this direction, the cyclotron mass of the holes is well separated from that of the electrons.

We then follow the angular variation of the hole cyclotron mass m_h^* by rotating the magnetic field carefully towards the trigonal direction. With this procedure we are able to identify the hole resonance lines in the neighborhood of the trigonal direction. Our results are shown in Fig. 10. Only two conditions are needed to fix the inverse effective masses in the hole Fermi surface (4) since $\beta_1=\beta_2$. The following observed hole cyclotron masses are used:

H along trigonal axis:

$$m_h^*=0.067\pm0.007m_0. \quad (24)$$

H along bisectrix axis:

$$m_h^*=0.226\pm0.02m_0. \quad (25)$$

Analogous to (22), angular variation of m_h^* in the present case is given by

$$m_h^*/m_0=(\sin^2\theta\beta_1\beta_3+\cos^2\theta\beta_1^2)^{-1/2}. \quad (26)$$

Here θ is the angle between H and the trigonal axis. From the values given in (24) and (25), we have determined that

$$\beta_1=\beta_2=14.8, \quad \beta_3=1.32. \quad (27)$$

These values are then used in (26) to calculate the angular variation of m_h^*. The computed curve is shown in Fig. 10. The agreement with the observed values is quite satisfactory.

2. H in the Bisectrix Plane

A. Electrons

When H is in the bisectrix plane, no analytic form for m^* can be obtained from the NENP model. We, thus, compare our results with the EP model. Since we have shown that α_2 is much smaller than α_1 and α_3, the EP model is a good approximation when p_2 is small. This is

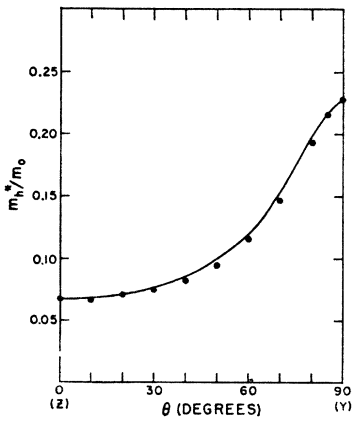

FIG. 10. Angular variation of the light-hole cyclotron mass with H in the binary plane. θ is the angle between H and the trigonal direction. The curve is a plot of Eq. (26) using $\beta_1=\beta_2=14.8$ and $\beta_3=1.32$.

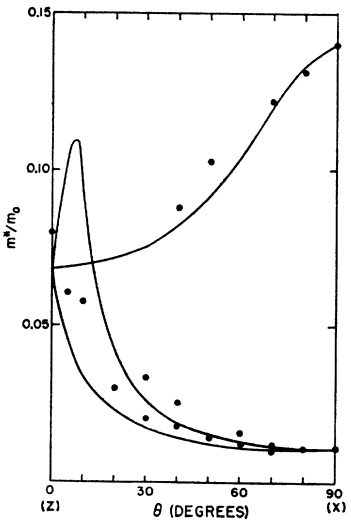

FIG. 11. Angular variation of the electron cyclotron mass with H in the bisectrix plane. θ is the angle between H and the trigonal direction. The solid lines are calculated from the EP model using (1) and (15).

the situation when H is nearly parallel to axis 2 and has been shown by Table I. In the present case, with H nearly perpendicular to axis 2, we would expect to see deviations from the EP model.

Using the reciprocal mass parameters obtained in (15), we have calculated values of m^* for the three ellipsoids from (1). The results are plotted in Fig. 11. As was also found in the previous case, the EP model gives m^* too small compared with the experimental values. The fairly good agreement observed in the neighborhood of the binary direction is partially due to the fact that the calculated value of m^* was chosen to fit the experimental point for that particular direction. Deviations from the EP model for H in the other directions are observed as expected.

B. Holes

The same orientation studies as were done with H in the binary plane were carried out for the hole cyclotron masses with H in the bisectrix plane. Again good agreement with the experimental data was obtained by using the spheroidal model with the inverse effective masses determined in (27). These results are plotted in Fig. 12, where the solid curve is the same as that of Fig. 10.

3. H in the Trigonal Plane

A. Electrons

The NENP model, owing to its complexity, gives no analytical expression for m^* in this orientation; thus, we use the EP model to fit our data. In this case, the experimental points are in almost perfect agreement with the theoretical curves derived from the EP model. This is the particular case in which the EP model enjoys great success.

The three curves shown in Fig. 13 are calculated from Eqs. (1) and (15). The observed values of m^* are shown to be fitted very well by these curves. Small deviations for H in the vicinity of the binary direction are observed. It can be seen from Fig. 13 that the observed points at $\theta=20°$, 40°, 80°, 85° are not fitted as well as those at other angles. Those small disagreements may also reveal a deviation of the electron Fermi surface from the EP model.

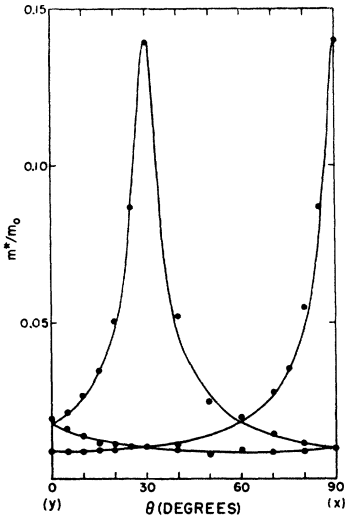

FIG. 13. Angular variation of the electron cyclotron mass with H in the trigonal plane. θ is the angle between H and the bisectrix direction. The solid lines are calculated from the EP model using (1) and (15).

B. Holes

Within the experimental accuracy, the hole cyclotron mass is shown to be unchanged when H is rotated from the binary direction to the bisectrix direction. This behavior of m_h^* is shown in Fig. 14.

From these constant values of m_h^*, and the same angular variation with H in the binary and bisectrix planes as shown in Figs. 10 and 12, we now come to the conclusion that the light hole Fermi surface is, indeed, of spheroidal shape with its long axis directed along the trigonal axis.

Using the values given by (27), we calculate the density-of-state mass of the light hole to be

$$M_h=0.15m_0. \tag{28}$$

Our results cannot determine the hole Fermi energy E_h. Using Brandt's[26] value of the extremal cross-section area and our values of the hole cyclotron masses, we

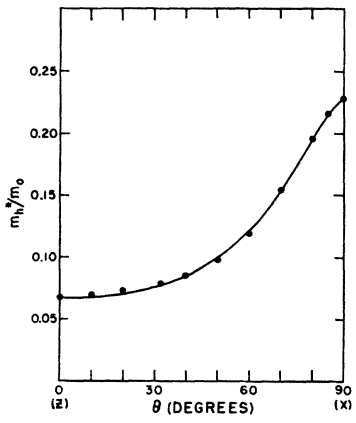

FIG. 12. Angular variation of the light-hole cyclotron mass with H in the bisectrix plane. θ is the angle between H and the trigonal axis. The curve is a plot of Eq. (26) using $\beta_1=\beta_2=14.8$ and $\beta_3=1.32$.

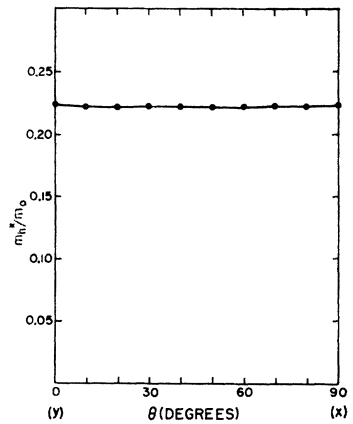

FIG. 14. Angular variation of the light-hole cyclotron mass with H in the trigonal plane. θ is the angle between H and the bisectrix axis.

TABLE II. Comparison of m^*/m_0 obtained by other cyclotron resonance experiments with the corresponding values observed in the present work.

	$H\|\|$binary axis			$H\|\|$bisectrix axis			$H\|\|$trigonal axis	
	Electrons		Holes	Electrons		Holes	Electrons	Holes
Source	m_I^*	m_{II}^*, m_{III}^*	m_h^*	m_I^*	m_{II}^*, m_{III}^*	m_h^*	m_I^*, m_{II}^*, m_{III}^*	m_h^*
Aubrey[a]	0.119	0.009	0.15	0.0078	0.0156	0.15	~0.06	~0.04
Galt *et al.*[b]	0.13	0.0105	0.25	0.0091	0.0180	0.25	0.08	0.068
Present work	0.14	0.0107	0.226	0.0091	0.0196	0.226	0.081	0.067

[a] See reference 12.

[b] See reference 13.

obtain the value of $E_h=0.012\pm0.002$ eV by assuming a parabolic valence band which is reasonable.

Cyclotron masses for the electrons and the light holes obtained by other cyclotron resonance experiments are listed in Table II in comparison with the corresponding values determined by the present work.

C. Dielectric Anomalies

The absorption peaks at ~500 G with H in the trigonal plane (Figs. 4 and 5) can be interpreted as "dielectric anomalies." The presence of these absorption peaks has also been observed in other cyclotron resonance experiments in Bi at different frequencies.[12,13]

This behavior in Bi can be qualitatively explained by the classical magneto-ionic theory. When a plasma containing more than one kind of carriers of the same sign but with different charge-to-mass ratios is in the presence of a dc magnetic field and high-frequency electromagnetic waves, cancellation of the total dielectric constant will take place depending upon the concentration and cyclotron frequencies of these charge carriers. This gives rise to a large power absorption when the dielectric constant becomes small. However, for a plasma in solid Bi at low temperatures, the classical theory is unable to calculate the exact position of this absorption peak because of the complication due to the anomalous skin effects.

With H in the trigonal plane, the EP model has been used successfully to identify every resonance line expected from the electrons and the holes as shown in Fig. 13. We may associate the remaining absorption peaks, which are not explained by the EP model, with the dielectric anomalies. We have found that the position of this particular absorption line remains almost unchanged when H is rotated in the trigonal plane.

Using this interpretation, we have identified all absorption peaks with H in the trigonal plane. For H in the other two planes, because of the complexity of the NENP model and the inaccuracy in the EP model, some absorption peaks cannot be interpreted unambiguously. Identification of the dielectric anomalies in those cases becomes difficult.

4. Number of Ellipsoids

From the values of m_1, m_2, and m_3 determined in Eq. (19) for the NENP model, we can calculate the total volume in momentum space enclosed by one "ellipsoid" from

$$V_e=(8\pi/3)(2m_1m_2m_3)^{1/2}E^{3/2}(1+6E/5E_g). \quad (29)$$

Using values of $E=0.022$ eV and $E/E_g=0.50$ as determined by other experiments,[14] we obtain the following value of the electron concentration per "ellipsoid":

$$n_e=2V/h^3=(1.29\pm0.2)\times10^{17}/\text{cm}^3. \quad (30)$$

In the EP model, we have

$$V_e=(4\pi/3)(2m_0E)^{3/2}(\alpha_1\alpha_2\alpha_3)^{-1/2};$$

with values of the α's given by (13) and $E=0.022$ eV,[27] we obtain

$$n_e=(1.35\pm0.2)\times10^{17}/\text{cm}^3. \quad (31)$$

Comparing either value of n_e obtained here with the total electron concentration N per cm^3 deduced by Jain and Koenig[17]:

$$N=3.9\times10^{17}/\text{cm}^3, \quad (32)$$

we see that there can only be three ellipsoids for the electrons in Bi as has already been shown by Jain and Koenig.

We calculate the hole concentration by using the values determined in (27) and the following expression for volume in momentum space:

$$V_h=(4\pi/3)(2m_0E_h)^{3/2}(\beta_1^2\beta_3)^{-1/2},$$

with $E_h=0.012$ eV, we obtain

$$n_h=(3.5\pm0.4)\times10^{17}/\text{cm}^3. \quad (33)$$

Comparison of (32) with (33) indicates that there can only be one spheroid for the light-hole Fermi surface. This result also reveals the possibility of the existence of another hole band with perhaps 10% as many holes in order to maintain charge neutrality by assuming there is only one electron band as we have discussed before.

[25] G. E. Smith, J. K. Galt, and F. R. Merritt, Phys. Rev. Letters, 4, 276 (1960).

[26] N. B. Brandt, Soviet Phys.—JETP 11, 975 (1960).

[27] D. H. Reneker, Phys. Rev. 115, 303 (1959).

TABLE III. Comparison of de Haas-van Alphen data[a] with the NENP model using the mass parameters determined in (19).

		Calculated value	Observed value[a]
H 78° from trigonal	Cyclotron mass	$0.0092m_0$	$0.0088m_0$
	dHvA period	7.6×10^{-5} G^{-1}	7.8×10^{-5} G^{-1}
H 168° from trigonal	Cyclotron mass	$0.029m_0$	$0.025m_0$
	dHvA period	2.5×10^{-5} G^{-1}	2.75×10^{-5} G^{-1}

[a] See reference 14.

5. Comparison with the de Haas-van Alphen Effect Data

In order to demonstrate the consistency of our determination of the mass parameters in the NENP model, we now use the values of m_1, m_2, and m_3 determined in (19) to calculate the values of the cyclotron mass and the dHvA period in pure Bi to make a comparison with the corresponding values observed in the dHvA effect experiments by Weiner.[14]

In the principal axis system, Weiner[14] observed the dHvA oscillations for two directions of the magnetic field in the binary plane and making angles 78° and 168°, respectively, with the trigonal axis. Referring to Fig. 9, since the solid curve is symmetric with respect to axis 3, these two directions correspond to $\theta=18°$ and $\theta=72°$, respectively. Results of our calculation are listed in Table III together with Weiner's observed values, the agreement is reasonably good.

ACKNOWLEDGMENTS

The author wishes to express his gratitude to Dr. S. H. Koenig for suggesting this research and for continued interest and encouragement, to Dr. J. I. Budnick and Dr. A. G. Redfield for many enlightening suggestions, to Dr. P. B. Miller, Dr. J. J. Hall, A. N. Friedman, and J. Kirsch for fruitful discussions. He is also indebted to Mrs. C. Pfister for examining the Bi crystal and to E. Boyd, W. Fite, II, and B. Mecs for technical assistance.

APPENDIX A

Let a be the area of intersection with a plane through axis 1 of the surface described by (3) and denote the angle between this plane and axis 2 by θ_1, then it can be shown that

$$a=\frac{4\cos^2\theta_1}{2m_2E_g}(2m_1E_g)^{1/2}\int_0^{\mu}[(t^2+\lambda^2)(\mu^2-t^2)]^{1/2}dt, \quad \text{(A1)}$$

where

$$\mu^2=(b_1^{1/2}-\nu_1)2m_2E_g/\cos^2\theta_1, \quad \text{(A2)}$$

$$\lambda^2=(b_1^{1/2}+\nu_1)2m_2E_g/\cos^2\theta_1, \quad \text{(A3)}$$

$$b_1=(E/E_g)(E/E_g+1)+\nu_1^2, \quad \text{(A4)}$$

$$\nu_1=\tfrac{1}{2}[1+(m_2/m_3)\tan^2\theta_1]. \quad \text{(A5)}$$

The following relation is useful:

$$I=\int_0^1 x^2\left(\frac{1-k^2x^2}{1-x^2}\right)^{1/2}dx=\frac{1}{3}\left[\frac{1-k^2}{k^2}K(k)+\frac{2k^2-1}{k^2}\epsilon(k)\right],$$

where

$$K(k)=\int_0^{\pi/2}\frac{d\varphi}{(1-k^2\sin^2\varphi)^{1/2}}$$

and

$$\epsilon(k)=\int_0^{\pi/2}d\varphi\,(1-k^2\sin^2\varphi)^{1/2}$$

are elliptic integrals of the first and second kinds. Let

$$k^2=\mu^2/(\mu^2+\lambda^2), \quad t^2=\mu^2(1-x^2);$$

we obtain

$$a=(4\cos^2\theta_1/2m_2E_g)(2m_1E_g)^{1/2}(\mu^3/k)I. \quad \text{(A6)}$$

Taking the derivative of (A6), we get

$$\frac{\partial a}{\partial E}=\frac{4(m_1m_2)^{1/2}}{\cos\theta_1}\left(1+\frac{2E}{E_g}\right)(2b_1^{1/2})^{-1/2}K\left(\frac{1}{(1+\tau_1)^{1/2}}\right). \quad \text{(A7)}$$

where

$$\tau_1=(b_1^{1/2}+\nu_1)/(b_1^{1/2}-\nu_1);$$

thus the cyclotron mass m^* for the present case can be written as

$$m^*=(2/\pi)(1+2E/E_g)(m_1m_2/2)^{1/2}G(\theta_1), \quad \text{(A8)}$$

where

$$G(\theta_1)=(\cos\theta_1b_1^{1/4})^{-1}K\left(\frac{1}{(1+\tau_1)^{1/2}}\right)$$

and

$$G(\pi/2)=(\pi/2)(2m_3/m_2)^{1/2},$$

when $\nu_1^2\gg(E/E_g)(E/E_g+1)$, (A8) reduces to

$$m^*=\left(1+\frac{2E}{E_g}\right)\left(\frac{m_1m_2m_3}{m_3\cos^2\theta_1+m_2\sin^2\theta_1}\right)^{1/2}. \quad \text{(A9)}$$

Similarly, for a plane through axis 3 making an angle θ_3 with axis 2, we obtain

$$m^*=(2/\pi)(1+2E/E_g)(m_2m_3/2)^{1/2}F(\theta_3), \quad \text{(A10)}$$

where

$$F(\theta_3)=(\cos\theta_3b_3^{1/4})^{-1}K\left(\frac{1}{(1+\tau_3)^{1/2}}\right),$$

$$b_3=(E/E_g)(1+E/E_g)+\nu_3^2,$$

$$\nu_3=\tfrac{1}{2}[1+(m_2/m_1)\tan^2\theta_3],$$

$$\tau_3=(b_3^{1/2}+\nu_3)/(b_3^{1/2}-\nu_3),$$

and $F(0)=G(0)$.